

Crashworthiness Simulation of Composite Automotive Structures

Mark Botkin
Nancy Johnson
Ed Zywicz
Srdan Simunovic

This paper was prepared for submittal to
13th Annual Engineering Society of Detroit Advanced
Composites Technology Conference and Exposition
Detroit, Michigan
September 28-29, 1998

June 1, 1998



Lawrence
Livermore
National
Laboratory

This is a preprint of a paper intended for publication in a journal or proceedings. Since changes may be made before publication, this preprint is made available with the understanding that it will not be cited or reproduced without the permission of the author.

DISCLAIMER

This document was prepared as an account of work sponsored by an agency of the United States Government. Neither the United States Government nor the University of California nor any of their employees, makes any warranty, express or implied, or assumes any legal liability or responsibility for the accuracy, completeness, or usefulness of any information, apparatus, product, or process disclosed, or represents that its use would not infringe privately owned rights. Reference herein to any specific commercial product, process, or service by trade name, trademark, manufacturer, or otherwise, does not necessarily constitute or imply its endorsement, recommendation, or favoring by the United States Government or the University of California. The views and opinions of authors expressed herein do not necessarily state or reflect those of the United States Government or the University of California, and shall not be used for advertising or product endorsement purposes.

GM NON-CLASSIFIED

Crashworthiness Simulation of Composite Automotive Structures

**Mark E. Botkin
Nancy L. Johnson**
Body Engineering & Integration Department

Ed Zywicz
Lawrence Livermore National Laboratory

Srdan Simunovic
Oak Ridge National Laboratory

June 25, 1998

Synopsis or Abbreviated Abstract

Damage models have been developed for crashworthiness of composite structures. The models have been implemented into a computer code and verified with test data.

Intended Audience (for presentation at the 13th Annual Engineering Society of Detroit Advanced Composites Technology Conference and Exposition, Detroit, Michigan, September 28-29, 1998,

CRASHWORTHINESS SIMULATION OF COMPOSITE AUTOMOTIVE STRUCTURES

Mark Botkin and Nancy Johnson, General Motors Corporation/ACC
Ed Zywicz, Lawrence Livermore National Laboratory
Srdan Simunovic, Oak Ridge National Laboratory

ABSTRACT

In 1990 the Automotive Composites Consortium (ACC) began the investigation of crashworthiness simulation methods for composite materials. A contract was given to Livermore Software Technology Corporation (LSTC) to implement a new damage model in LS-DYNA3D™ specifically for composite structures. This model is in LS-DYNA3D™ and is in use by the ACC partners. In 1994 USCAR, a partnership of American auto companies, entered into a partnership called SCAAP (Super Computing Automotive Applications Partnership) for the express purpose of working with the National Labs on computational oriented research. A CRADA (Cooperative Research and Development Agreement) was signed with Lawrence Livermore National Laboratory, Oak Ridge National Laboratory, Sandia National Laboratory, Argonne National Laboratory, and Los Alamos National Laboratory to work in three distinctly different technical areas, one of which was composites material modeling for crashworthiness. Each Laboratory was assigned a specific modeling task. The ACC was responsible for the technical direction of the composites project and provided all test data for code verification. All new models were to be implemented in DYNA3D and periodically distributed to all partners for testing. Several new models have been developed and implemented. Excellent agreement has been shown between tube crush simulation and experiments.

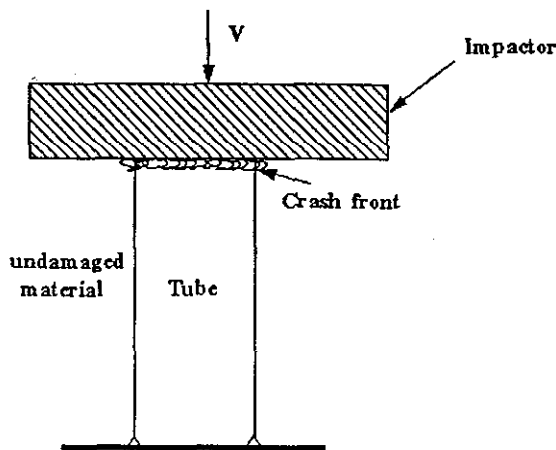
INTRODUCTION

The Automotive Composites Consortium has been working in automotive crashworthiness since 1988¹. A major accomplishment came in 1996 with a successful composite vehicle crash test². Although this was a successful project, the development time could have been shortened by having a computational method for crashworthiness. Work in this area has been limited largely due to the lack of a broad-based application, since post-failure analysis of composites is primarily a concern of the auto industry. The investigation by Oehmke³ on crush of tubes with uni-directional lay-ups showed the Chang-Chang model⁴ to be of limited usefulness. In 1990 the ACC sponsored work to develop a new composites damage model^{5,6}. That project resulted in reasonable correlation, but was also limited to tubes with uni-directional lay-ups. Other similar work focused on sandwich construction⁷. More recently, Kerth has shown good agreement with tests of thermoplastic composite tubes of a *double hat* configuration⁸.

It was felt that any additional work must be focused on reinforcement types that are commonly used in production applications. For that reason, the work plan for the SCAAP CRADA included an emphasis on braided and CSM (continuous strand mat) preforms.

LS-DYNA3D™ MODEL 58^{5,6}

Analytical methods to predict the post-failure dynamic response of polymer composite materials are needed by the automotive industry to reduce the time required for design development. A damage model was implemented in LS-DYNA3D™ for the ACC



to predict the axial crush response of composite tubular members. The composite laminate is assumed to be made from unidirectional laminae or plies in which the fiber directions of each ply are uniquely specified. The composite members are modeled using triangular and quadrilateral shell elements which have multiple integration points through the thickness. Ply thickness, fiber orientation, and constitutive constants are required as input by the user.

Figure 1 Crush of a typical Tube

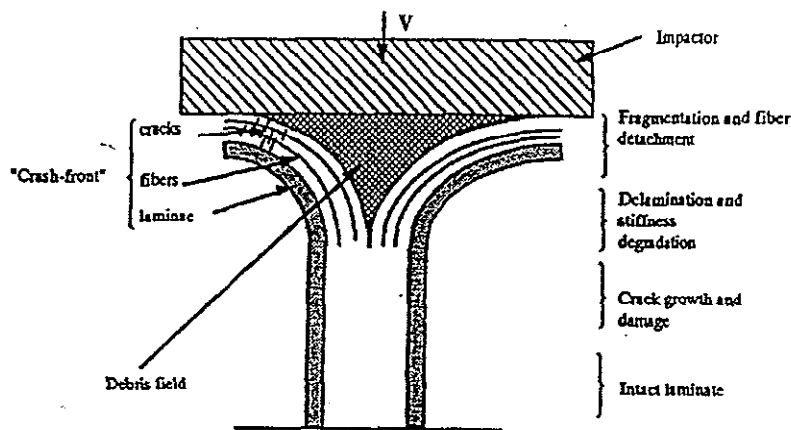
Crush of a typical energy absorber consists of a pair of square tubes attached between the bumper and the chassis of a vehicle. During the event, the

tube crushes progressively and dissipates energy. A representative diagram of the axial crush of a composite tube using an impactor is shown in Figure 1, with the crush front area identified.

Before developing the new composite damage model, an investigation of previously developed damage models was completed to determine their applicability to composites. Different types of failure mechanisms for composites include:

1. Transverse matrix cracking
2. Transverse matrix crushing
3. Fiber breakage
4. Fiber buckling and matrix crushing in the fiber direction
5. Delamination
6. Debonding between fiber and matrix.

These different failure mechanisms are shown in Figure 2. For this study, delamination and debonding were not considered.



In this section, an overview of the composite damage model will be provided, followed by results from a test problem. The composite beam in the first test problem is a square, composite beam with thick walls and rounded corners.

Figure 2 Failure Mechanisms in Crush of Composite Tubes

Composite Damage Model

A co-rotational stress update was outlined by Belytschko and co-workers^{9,10} for all shell element formulations with the exception of the Hughes-Liu shell^{11,12,13}. In these formulations the stresses are stored and updated in the orthogonal co-rotational coordinate system that is defined by the 1-2 element side and the cross product of the diagonals. The transformation of the stress and strain tensors into the local system determined by the fiber directions in the ply takes place in the plane of the shell. In the application of the shells to layered composite laminates it is normal to store one stress tensor per integration point and to use one integration point per ply.

Since each ply in the laminate may have unique fiber orientations, a method is provided for specifying the orientation angles. The angle ψ shown in Figure 3 is uniquely defined for each shell element either by specifying ψ on the element definition card or by letting LS-DYNA3D™ automatically determine the orientation of a and therefore, ψ , by some global reference specified in the input, e.g., that a is parallel with the global x axis. Each ply requires the specification of the orientation angle, β , in the material input which positions the fiber relative to a . Then the orientation of the fiber direction in each ply is found by the summation of $\beta + \psi$ as shown in Figure 3.

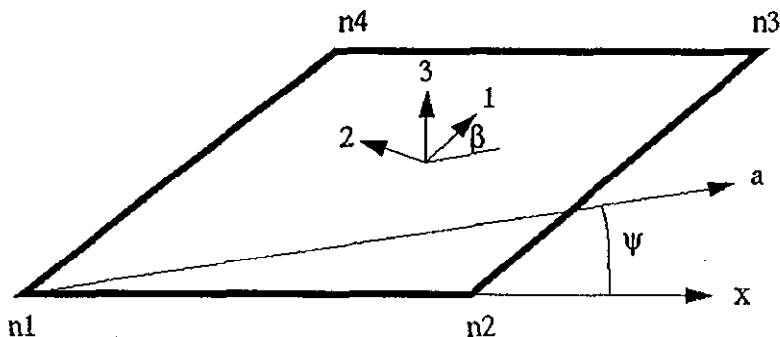


Figure 3 Orientation of Material Directions Relative to the 1-2 Side

The composite damage model represents an extension of continuum damage mechanics¹⁴ and includes independent damage parameters for tensile and compressive failure in the longitudinal and transverse directions. There is also a damage parameter for shearing in the plane of the shell.

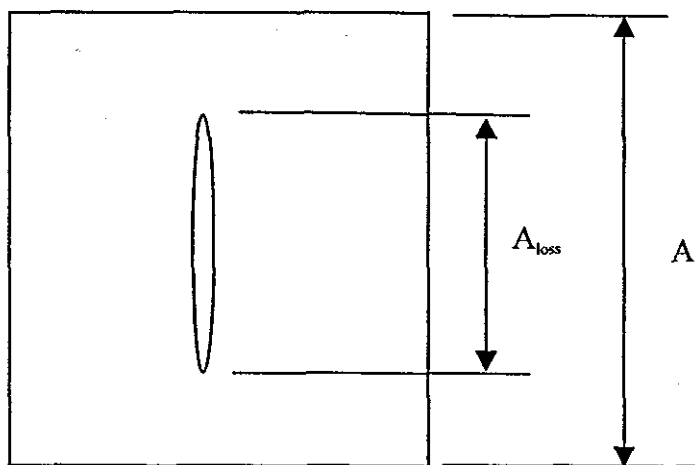


Figure 4 Crack in a Volume Element

The classic concept of damage mechanics is based on the uniaxial model shown in Figure 4. The damage is measured by the parameter, ω , which is defined as the ratio of the lost area due to damage over the total area: $\omega = A_{\text{loss}}/A$ where $0 \leq \omega \leq 1$. Values of $\omega = 0$ and $\omega = 1$ indicate no damage and complete damage, respectively. Young's modulus for the damaged material is defined as: $E(\omega) = \sigma/\epsilon = (1 - \omega)E$. This definition for the modulus of the damaged

material leads to the physical interpretation of *damage as the degradation of the elastic material stiffness*.

First, in order to show how the constitutive equations are derived, the isotropic case will be shown and then extended to the orthotropic case. From the above definition of Young's modulus of the damaged material, the modulus in the direction of the crack normal is given by $E_{\parallel} = (1-\omega) E$. Similarly, the shear modulus of the damaged material is $G(\omega) = (1-\omega) G$. In classical damage mechanics it is assumed that damage does not affect elasticity in the transverse direction, ie, $E_{\perp} = E = \text{constant}$. Therefore, the constitutive law for plane stress of the isotropic case can be expressed as:

$$\begin{bmatrix} \varepsilon_{\parallel} \\ \varepsilon_{\perp} \\ \gamma \end{bmatrix} = \begin{bmatrix} \frac{1}{(1-\omega)E} & -\nu/E & 0 \\ -\nu/E & 1/E & 0 \\ 0 & 0 & \frac{1}{(1-\omega)G} \end{bmatrix} \begin{bmatrix} \sigma_{\parallel} \\ \sigma_{\perp} \\ \tau \end{bmatrix}$$

For the orthotropic case, where cracks are parallel to the fibers, it is assumed that E_{22} degrades as a function of ω , such that: $E_{22} = (1-\omega) E_{\perp}$ and that $E_{11} = E_{\parallel}$. Similar calculations can be done for the case where the cracks are orthogonal to the fibers.

For the general case where cracks are modeled as two orthogonal sets of crack arrays, the following constitutive law is obtained:

$$\begin{bmatrix} \sigma_{\parallel} \\ \sigma_{\perp} \\ \tau \end{bmatrix} = \frac{1}{c} \begin{bmatrix} (1-\omega_{\parallel})E_{\parallel} & (1-\omega_{\parallel})(1-\omega_{\perp})\nu_{21}^0 E_{\parallel} & 0 \\ (1-\omega_{\parallel})(1-\omega_{\perp})\nu_{12}^0 E_{\parallel} & (1-\omega_{\perp})E_{\perp} & 0 \\ 0 & 0 & c(1-\omega_s)G \end{bmatrix} \begin{bmatrix} \varepsilon_{\parallel} \\ \varepsilon_{\perp} \\ \gamma \end{bmatrix}$$

The parameters ω_{\parallel} , ω_{\perp} , and ω_s are calculated from the damage evolution law which is related to the Weibull distribution:

$$\omega = 1 - \varepsilon^{-\left(\frac{\varepsilon}{\varepsilon_0}\right)^m}$$

where m and ε_0 are two independent parameters to describe damage. By selecting the appropriate values for the damage parameters, m_{\parallel} , m_{\perp} , $m_{\perp c}$, $m_{\perp c}$, and m_s , a stress-strain curve can be obtained which is representative of those obtained experimentally.

Examples of curves corresponding to various values of m are shown in Figure 5. The m values are required as input parameters to the program.

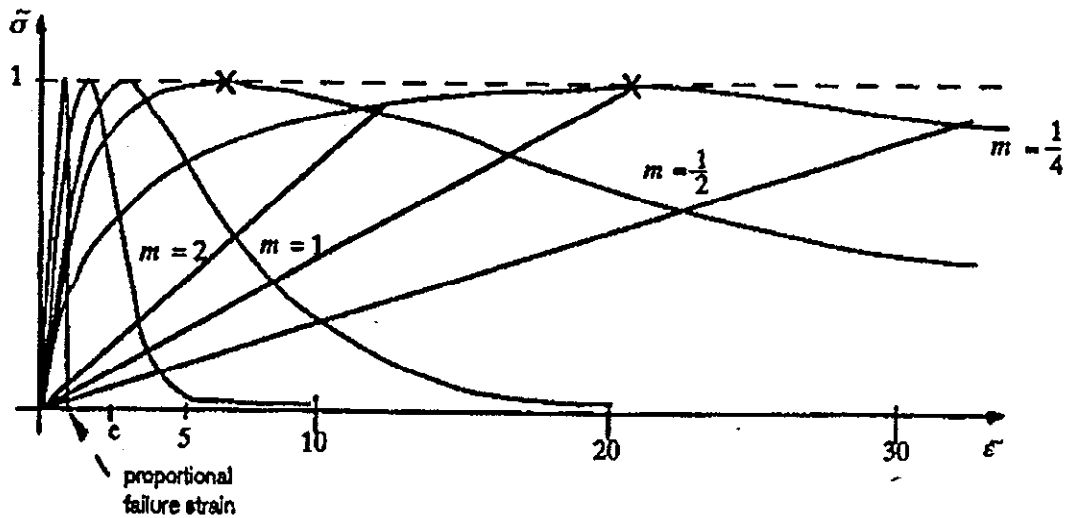
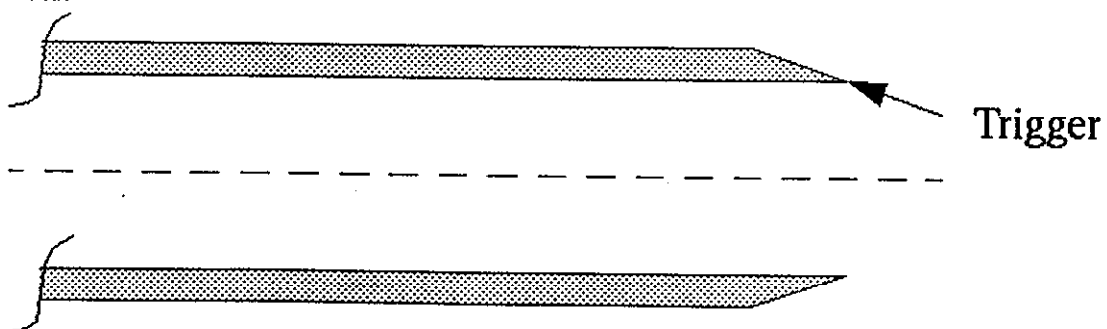


Figure 5 Examples of Stress-strain Curves for Various Values of m

Crash-Front Modeling

The zone of crushed, fragmenting material which develops as crush progresses along the tube is called the crash-front. Often a trigger, such as a chamfer as shown in Figure 6 creates a region of high stresses which initiates failure. Immediately in front of the crash-front zone, cracks propagate into yet undamaged material limiting the ability of the cracked material to transmit stresses high enough to cause failures away from the crash-front.

By weakening the materials in the crash-front, the stresses are limited to values that are less than the values required to fail the material. Figure 7 demonstrates the crash-front in the finite element model. The failure strength of these elements will be reduced by a factor, *soft*, and the factor, *fbrt*, which reduces the tensile strength of the fiber. The failure criterion is based on a limiting time step size such that if the time step size for an element falls below a minimum size defined by the user, *tsize*, then the element is assumed to have failed and is removed. The parameters *soft*, *fbrt*, and *tsize* are input by the user.



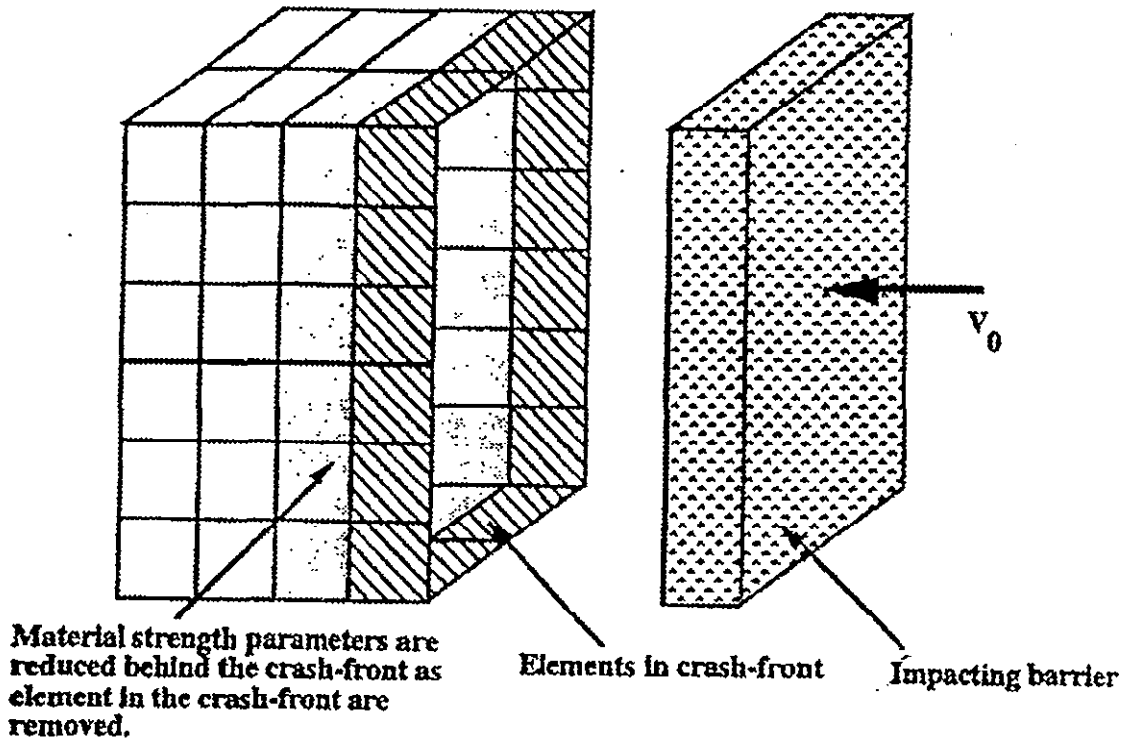


Figure 7 Crash Front Propogates Through Tube

Results

The square tube shown in Figure. 8 was used as a verification test case and was taken from Ref. 3. The model consists of 1368 four-noded quadrilateral elements connecting 1404 nodes. The elements are nominally 10mm square. The tube is 90mm square (outer dimension) and 375mm long. The outside corner radius is 16mm and the thickness is 5mm. The fiber orientation is 90/0/-45/45 of fiberglass material. The material properties are shown in Table I. The tube was tested in a drop silo using a 220.6 kg mass and an impact velocity of 12.5 m/sec.

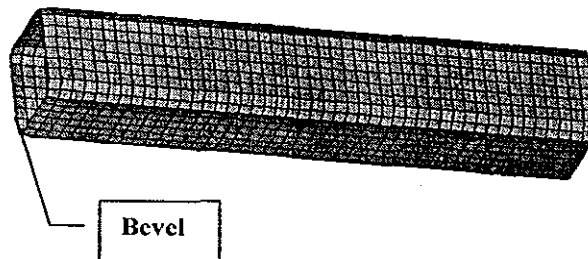


Figure 8 Undeformed tube mesh

Table I Ply Material Properties for Composite Tube

$E_1 = 14.3 \text{ kN/mm}^2$	$G_{12} = 3.31 \text{ kN/mm}^2$
$E_2 = E_3 = 3.65 \text{ kN/mm}^2$	$\sigma_{t1} = .318 \text{ kN/mm}^2$
$\nu_{21} = .08$	$\sigma_{t2} = .0236 \text{ kN/mm}^2$
$\nu_{23} = .08$	$\sigma_{e1} = .318 \text{ kN/mm}^2$
$\nu_{31} = .321$	$\sigma_{e2} = .111 \text{ kN/mm}^2$
$\rho = 1.8 \times 10^{-6} \text{ kg/mm}^3$	$\tau_{\text{max}} = .6559 \text{ kN/mm}^2$

The damage parameters used in the analysis were: $m_{11c} = 0.5$, $m_{11t} = 3.0$, $m_{22c} = 0.5$, $m_{22t} = 2.0$, and $m_s = 0.5$. The crash-front parameters were: $t_{\text{size}} = 0.20\text{e-}03$, $\text{soft} = 1.0$, and $\text{fbrt} = 1.0$.

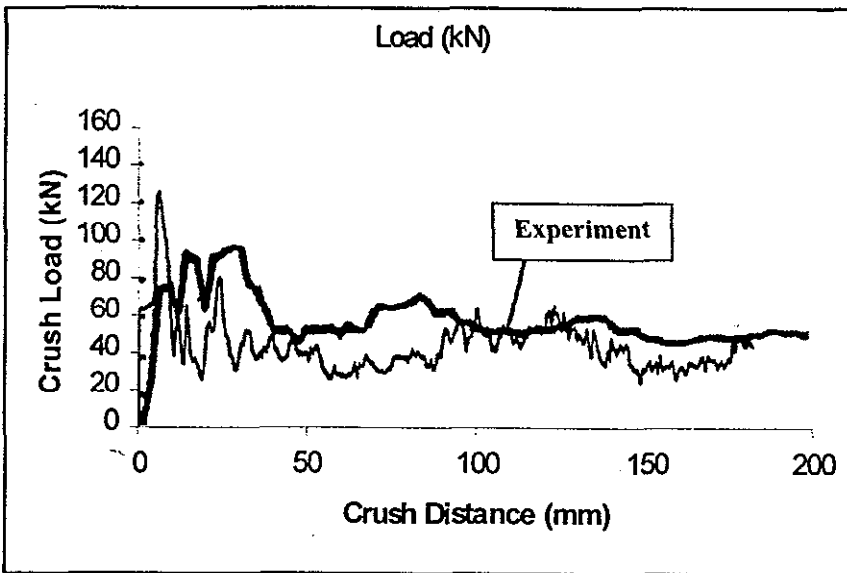


Figure 9 Force-Displacement Results for Model 58

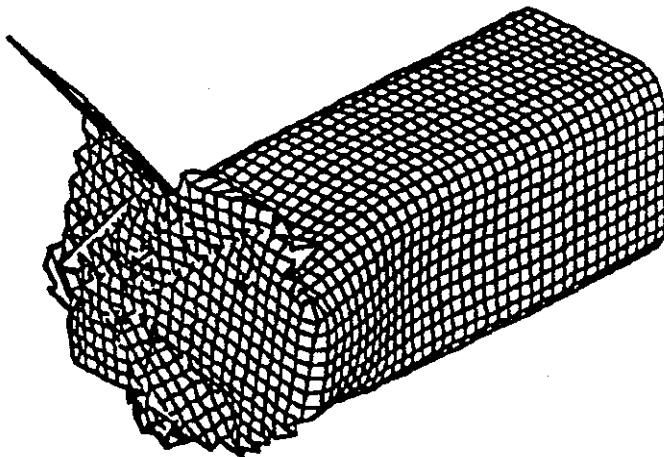


Figure 10 Deformed shape for Model 58

The deformation of the beam and the crush load-crush distance curve are shown in Figures 9 and 10, respectively. The average crush load is about 50 kN which compares favorably with the experimental data. The deformed plot shows the mesh to be quite distorted to the point that it is difficult to determine a failure mode, possibly indicating that such models may be *tuned* to produce acceptable force levels but may not actually represent reality.

SCAAP MODELS

The following models were developed as part of the SCAAP CRADA, as indicated above, in an effort to extend the modeling capability to fiber architectures typical of those used in automotive manufacturing.

Braid Damage Model

Automotive structures manufactured from braided composites demonstrate a multitude of complex and interdependent inelastic behaviors and failure mechanisms when crushed during vehicle impacts. A plane-stress constitutive model has been developed to replicate the behavior of these materials in crashworthiness simulations. The orthotropic models are intended for use in co-rotational shell elements and address the predominate deformation modes. It incorporates elasticity, anisotropic plasticity, and four directionally dependent tensile and compressive damage mechanisms to replicate the complex material behaviors experimentally observed. The model addresses only the deformation modes that result from inplane loading, but when coupled with other techniques, such as the newly developed delamination element¹⁵, it can efficiently and accurately predict the three-dimensional response of many automotive structures.

The braided composite constitutive relationship is developed using the thermodynamic framework employed by Hansen and Schreyer¹⁶ and Govindjee, et al.¹⁷, and it attempts to replicate the underlying micro-mechanical behaviors with a "smeared" lamina-level relationship. The law is expressed in a Cartesian coordinate system that is aligned with the principal roving direction (the 1-direction) and the shell normal (the 3-direction) and initially possesses orthotropic symmetry. Using reduced notation, the stress can be stated in terms of the instantaneous compliance, total strain, and plastic strain by

$$\boldsymbol{\sigma} = \boldsymbol{S}^{-1} (\boldsymbol{\epsilon} - \boldsymbol{\epsilon}^p), \quad \text{where } \boldsymbol{\sigma} = \begin{Bmatrix} \sigma_{11} \\ \sigma_{22} \\ \sigma_{12} \\ \sigma_{23} \\ \sigma_{13} \end{Bmatrix} \quad \text{and } \boldsymbol{\epsilon} = \begin{Bmatrix} \epsilon_{11} \\ \epsilon_{22} \\ \gamma_{12} \\ \gamma_{23} \\ \gamma_{13} \end{Bmatrix}.$$

During deformation, both the instantaneous compliance and plastic strain evolve, in a non-reversible manner, as functions of the internal damage variables.

Tensile Damage

The primary tensile damage mechanism is assumed to be the evolution of micro and macro cracks on planes perpendicular and parallel to the fibers. In general, three independent fiber directions exist in a braided composite, and therefore cracks may form in six different directions. However, for low angle symmetric braids, tensile damage can be reasonably approximated by resolving damage only on the planes parallel and

perpendicular to the principal roving direction. (Henceforth, quantities associated with the roving's parallel and perpendicular directions will be denoted with the superscripts 0 and 90, respectively.)

Damage is represented by enhancing the local material compliance in preferential directions. The amount and direction of enhancement contributed by "cracks" in each crack-plane direction is controlled by an evolving damage surface and an internal tensile damage variable t . Each damage surface is constructed by normalizing the traction vector on the postulated crack surface with \mathcal{M} , the crack-plane direction tensor, and equating the resultant with a damage function. In reduced form, the damage surfaces for the roving and transverse directions can be expressed simply as

$$\phi_t^0 = \left(\sigma_{11}^2 + \zeta_1^0 \sigma_{12}^2 + \zeta_2^0 \sigma_{13}^2 \right)^{1/2} \sigma_f^0 \exp \left(\frac{-t^0}{t_o^0} \right)$$

and

$$\phi_t^{90} = \left(\sigma_{22}^2 + \zeta_1^{90} \sigma_{12}^2 + \zeta_2^{90} \sigma_{23}^2 \right)^{1/2} \sigma_f^{90} \exp \left(\frac{-t^{90}}{t_o^{90}} \right),$$

respectively, where σ_f is the associated tensile strength, t_o controls the amount of energy dissipated (a material constant) and ζ are weighting factors (also material constants). Damage evolves when $\phi = 0$, and t must increase such that $\dot{\phi} \leq 0$. The equations that dictate how the compliance is enhanced are derived from the damage surfaces and a postulated energy potential (omitted for brevity) by enforcing the 2nd law of thermodynamics and maximizing the dissipational energy. The latter condition results in the direction of compliance enhancement being normal to the damage surface, i.e., in the \mathcal{M} direction. After some manipulation, the instantaneous material compliance \mathcal{S} is expressible as

$$\mathcal{S}(t_o^0, t_o^{90}) = \mathcal{S}_o + \mathcal{M}^0 \frac{\sigma_f^0}{t_o^0} \left[\exp \left(\frac{t^0}{t_o^0} \right) - 1 \right] + \mathcal{M}^{90} \frac{\sigma_f^{90}}{t_o^{90}} \left[\exp \left(\frac{t^{90}}{t_o^{90}} \right) - 1 \right],$$

where

$$\mathcal{M}^0 \equiv \begin{bmatrix} 1 & 0 & 0 & 0 & 0 \\ 0 & 0 & 0 & 0 & 0 \\ 0 & 0 & \zeta_1^0 & 0 & 0 \\ 0 & 0 & 0 & 0 & 0 \\ 0 & 0 & 0 & 0 & \zeta_2^0 \end{bmatrix}, \quad \mathcal{M}^{90} \equiv \begin{bmatrix} 0 & 0 & 0 & 0 & 0 \\ 0 & 1 & 0 & 0 & 0 \\ 0 & 0 & \zeta_1^{90} & 0 & 0 \\ 0 & 0 & 0 & \zeta_2^{90} & 0 \\ 0 & 0 & 0 & 0 & 0 \end{bmatrix},$$

and δ_0 is the initial compliance.

The tensile damage relationships derived above are consistent with 3-dimensional elastic fracture mechanics. The yield surfaces are parametrically similar to expressions that relate the remote applied stress levels to the initiation of unstable crack growth, e.g., a circular inclusion in an infinite solid subjected to far-field tractions. The present stress-based formulation results in compliance enhancement rather than stiffness degradation. This preserves the material symmetry and is consistent with micro-mechanical solutions of dilute, periodic, non-interacting co-planar elastic cracks and low to modest volume fractions of planar cracks as a function of crack density. For a simple 1-dimensional tension test, the constitutive relationship yields a bi-linear stress-strain response that smoothly transitions to zero stress.

Anisotropic Plasticity

Plasticity is included to emulate the nonlinear behavior observed under uniaxial transverse compression as well as inplane and through-the-thickness shear loadings. An anisotropic model is necessary since not only are the transverse and shear responses not multiplicatively related, but in braided composites, the axial response typically exhibits no non-linear behavior prior to peak load. To simulate this behavior, a yield surface is constructed from Hill's general anisotropic surface¹⁸ by imposing symmetry in the transverse/through-the-thickness plane and by setting the shear weighting factors in the through-the-thickness directions equal. The resulting plane-stress yield surface is given by

$$\phi_y = \alpha\sigma_{11}^2 + \delta\sigma_{22}^2 - \alpha\sigma_{11}\sigma_{22} + (4 + \alpha)\sigma_{23}^2 + \iota(\sigma_{12}^2 + \sigma_{13}^2) - G(\bar{\epsilon}^p),$$

where α and δ are weighting factors and ι is a material coefficient. Initially, $\alpha \ll 1$ and $\delta = 1$, but, as described later, these factors are varied to represent compressive damage. The function $G(\bar{\epsilon}^p)$ describes the transverse compressive response as a function of equivalent plastic strain, and is modeled with a power-law relationship of the form

$$G(\bar{\epsilon}^p) = \sigma_o \left(1 + \frac{\bar{\epsilon}^p}{\epsilon_o} \right)^n.$$

The necessary material constants for $G(\bar{\epsilon}^p)$ are obtained by curve fitting the transverse compressive response.

Using the yield surface and a postulated energy potential, enforcement of the 2nd law and the maximum dissipational energy assumption result in the evolution equations for the plastic strains and the requirement that $\bar{\epsilon}^p$ must increase so that $\phi_y \leq 0$. Similar to before, the maximum dissipational assumption requires that the plastic strain rate be

normal to the yield surface, i.e., be coaxial with the deviatoric stress. Thus, the resultant evolution equation for the plastic strains and the consistency conditions are identical to those of conventional J2 plasticity. Because only the yield surface and the definition of the deviatoric stresses differ, the same equations and approaches employed to update the plastic strains in conventional plane-stress plasticity relationships are used here as well.

Compressive Damage

Although several different mechanism usually control compressive failure, their homogenized responses at the macro level are often indistinguishable in braided composites. Typically, in uniaxial compression, a diffuse band of localized deformation forms normal to the direction of the applied load. Within this band appreciable fiber reorientation, kinking, and bowing occurs. While the development of the band reduces the load bearing capacity of the composite, it does not significantly reduce the composite's instantaneous elastic stiffness. Consequently, under uniaxial compressive conditions, the composite's post-peak response can be idealized by that of an elastic-plastic solid that strain softens, in the current loading direction, to a saturation value. The present model replicates this behavior by modifying α and δ in the yield surface based upon the internal damage variables c^0 and c^{90} , respectively. The damage variables are controlled by the strain-based fiber-direction and transverse/shear-direction damage surfaces, given by

$$\phi_c^0 = \left(\frac{\epsilon_{11}}{\epsilon_{11c}} - 1 \right) / c_o^0 - c^0$$

and

$$\phi_c^{90} = \left(\frac{\sqrt{(|\epsilon_{22}| - \epsilon_{22})\epsilon_{22} + \nu \gamma_{12}^2}}{\epsilon_{22c}} - 1 \right) / c_o^{90} - c^{90},$$

respectively. Here ϵ_c (the associated strain at peak compressive load), ν , c_o^{90} and c_o^0 are material constants, and c must evolve such that $\phi_c \leq 0$. As compressive damage evolves, c , initially zero, increases to its maximum value of unity and concurrently drives its associated weighting factor α or δ to its saturation limit. The equations that relate c^0 to α and c^{90} to δ (omitted for brevity), generate uniaxial post-peak compressive responses that decrease linearly with strain to a prescribed, fully-damaged, saturation stress.

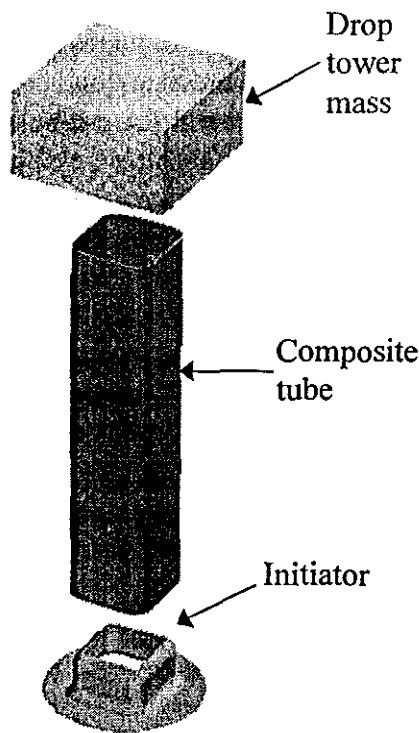
Overview

The present model has been validated with a multitude of controlled laboratory experiments, e.g., four-point bend tests, and actual component tests. Comparisons with

quasi-static uniaxial tension and compression tests performed at various fiber orientations demonstrate that the damage and plasticity surfaces in the model correctly capture the onset of inelastic deformation under multi-axial strain states. The tests also show that the anisotropic plasticity model accurately tracks the material as it strain hardens. The post-peak or "damage" regime has been probed via traditional three- and four-point bend tests as well as biased four-point bend tests. For select configurations, these tests remain stable over large portions of the loading range even as damage evolves, and thus are useful for both validation and inferring damage properties. However, the most relevant and important validation is how well the new technology can replicate impact conditions in actual automotive structures.

Tube Crush Example

The primary energy dissipation components in most passenger vehicles are the "rails." These tubular structures dissipate as much as 60% of the energy in frontal impacts. Composite tubes, similar in geometry to actual automotive rails, were dynamically tested in an instrumented drop-tower to evaluate their crush response. Drop-



tower simulations were then performed, and compared to the experimental results. Figure 11 shows the simulated test in an expanded configuration. The drop-tower mass is lumped into a single element attached to the top of the rail. The three-ply rail is modeled with three layers of concentric shell elements. Each layer of shell elements is connected to the next layer using eight-node delamination elements. The initiator, inserted in the bottom of the rail, helps regulate the force necessary to start crushing the rail. Located below the initiator is the load cell which is modeled as a mathematical rigid wall (not shown). In the simulation, an initial axial velocity is prescribed to all three components, and the force between the rigid wall and initiator is then recorded.

Figure 11 Undeformed Composite Tube, Initiator and Drop Tower Mass

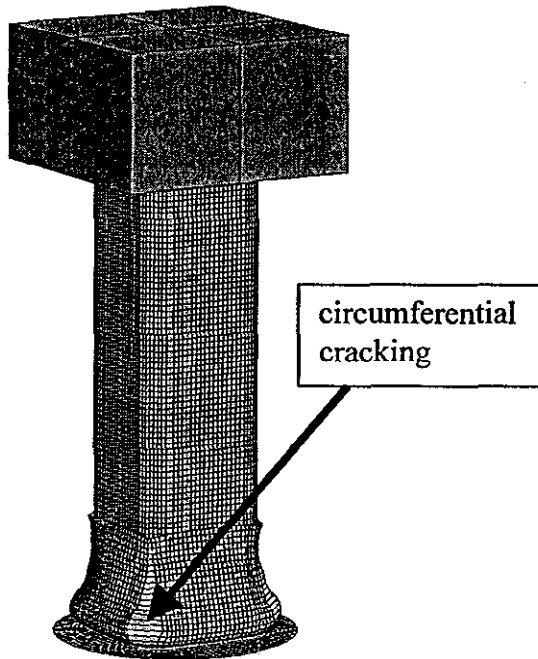


Figure 12 Deformed Crush Tube

Figure 12 shows the deformed geometry approximately 24 milliseconds into the 60 millisecond crush event. At this point the tube has rolled back upon itself. As can be seen by the *stretched* elements in the figure, extensive circumferential cracking develops especially at the corners. The extent of this circumferential cracking strongly influences the axial deformation since it controls how closely the rail follows the initiator radius. When the corner “crack tip” remains only a small distance above the initiator, the axial deformation mode is relatively smooth and yields a nearly constant axial resistance. As the steady-state crack length increases, the axial force and deformation mode become jagged and the rail splits into several

pronounced fronds. The bending of the fronds tends to localize at discrete intervals between nearly intact fragments. Generally speaking, the smaller the radius of curvature, the higher the axial force generated by the rail.

Plotted in Figure 13 are the simulated and experimentally recorded axial force versus time traces. Results from two different models are included. The trace labeled “New” was obtained using the newly developed material model and delamination elements. The other simulated trace, labeled “Traditional”, was obtained using the new material model, but with only one shell element through the composite thickness. Both simulations employed the same material constants and depicted the same tests. Clearly, the explicit incorporation of delamination better represents the physics present during this crush event.

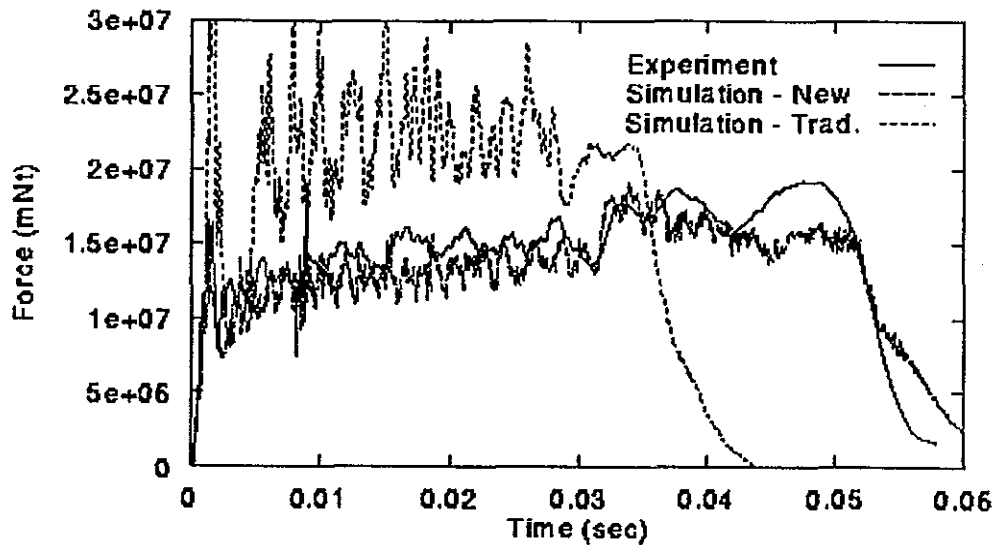
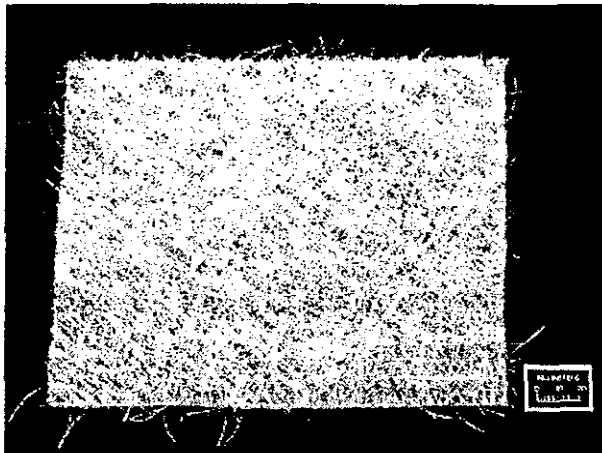


Figure 13 Comparison of Analysis with Test

Constitutive Modeling of Continuous Strand Mat Glass Fiber Polymer Composites

Background

The Continuous Strand Mat (CSM) glass fiber polymer composite is a relatively inexpensive composite material that is already widely used for structural applications in boat industry for boat hulls. The CSM composite is relatively simple to produce and does not require sophisticated layup and molding equipment. The low cost and excellent energy absorption properties during crushing make CSM a strong candidate for automotive impact energy absorption components. In this study, the CSM composite system was considered both for automotive structural components made entirely of CSM and for the external layers of hybrid laminates that incorporated woven or braided glass fibers.



(a)



(b)

Figure 14 (a) Single CSM Ply, (b) Five Plies, Side View

The continuous strand mat is fabricated from multiple strands of E-glass that are continuously deposited on a flat surface in a spiral fashion. In order to reduce the final cost, the strands are often supplied directly from the glass fiber manufacturing process. The desired weight of the mat is achieved either by controlling the number of strands that are simultaneously deposited or by passing the mat through multiple stages with a fixed number of strands. The result is a thick, springy, layered mat that can easily interlock with neighboring mats. A typical CSM ply and the side view of multiple CSM layers are shown in Figure 14. This interlocked structure makes delamination in CSM more difficult compared to more ordered fiber systems such as textiles and braids, and, therefore, favors the crushing mode of the material in axial impact. The mat manufacturing process, fiber sizing, and binder type and compatibility, all influence the structural deformation characteristics of the

CSM composite. A characteristic CSM used in this study was Vetrotex-CertainTeed Uniflo U-750 in weights of 1.5 and 2 oz/ft². The mats were produced with silane plastic sizing for promoting interface bonding with polymer resins used in this study (polyesters, vinyl esters, and epoxies) and with polyester powder binder to ease the handling of the mats. One third of its basic strand of 50 tex (tex is a unit for expressing linear density equal to the mass in grams of 1000 meters of strand) is situated in the center layer which facilitates resin impregnation to the mat's core. The CSM mats are more bulky compared to fabrics and are prone to composite manufacturing flaws such as voids and dry spots, as well as pinching of the mat by the molding equipment.

The thermoset polymer systems used for CSM composite matrices were: vinyl ester (Arotech Q6055, Ashland Chemical, Inc.), epoxy vinyl ester (Derakane 411-C-50, Dow Chemical Co.), and polyisocyanurate (Spectrim MM 364, Dow Chemical Co.). These resins have very similar mechanical properties but may develop different interface structures with glass fibers especially when a different composite manufacturing process is employed. The composites used in this study were manufactured using a resin transfer

molding (for Arotech and Derekane) and a structural reaction injection molding (for Spectrim) followed by varying degrees of cure and environmental influences.

Material Modeling

The deformation in the CSM composites can be generally observed in the three constituent phases: glass fiber, polymer matrix, and their interfaces. The ability to undergo plastic deformation in each of the constituents is extremely limited due to their brittle nature. The resulting deformation and energy dissipation during impact is achieved through creation of large areas of fracture. The fracture is not a single event but a process involving mutually interacting physical mechanisms such as: delamination, intralaminar matrix cracking, longitudinal matrix splitting, fiber/matrix debonding, fiber pull-out and fracture, etc. The damage processes in one phase may interact with damage from other phases depending on both intrinsic (material) and extrinsic (geometry, loading) effects. The rigorous micromechanical characterization and representation of all damage and failure processes in composite materials with complex microstructure such as CSM is beyond current computational capabilities. Moreover, difficulties associated with the determination and quantification of micromechanical model parameters would most likely offset any practical benefits of such a scientific venture.

Continuum damage models that relate to main deformation aspects of micromechanical processes are currently the only feasible approach for modeling of impact deformation in complex composite structures. The details on damage mechanics theory and formulations can be found in standard textbooks, such as Reference 19. During this study, several material models based on damage mechanics framework were developed. The energy dissipation mechanisms in the material were described by material internal variables, ω , that reflect average material degradation and damage evolution. Because of the nature of deformation and geometry of the structures that were modeled, all of the developed CSM composite models started from the following general assumptions:

1. All nonlinear effects of constitutive behavior are attributed to damage. Plastic deformations are negligible.
2. Unloading and reloading do not produce additional damage in the material.
3. Damage depends on the resulting tensile and compressive states.
4. The model is developed for shell structures for which the state of plane stress is prevalent.

Assumptions 1 and 2 restrict the functional dependence of the material's free energy as

$$\Psi = \Psi(\varepsilon, \omega) \quad (1)$$

where ε denotes a strain tensor and ω represents damage descriptors (variables). In the developed models, the unilateral nature of the damage has been modeled by expressing the free energy into separate parts that correspond to different damage mechanisms. Therefore, the energy associated with the particular damage mode and its evolution, can be identified and derived from Eq. (1).

Stress tensor is derived from the free energy as

$$\sigma = \frac{\delta \Psi (\varepsilon, \omega)}{\delta \varepsilon} \quad (2)$$

The associated thermodynamics force to damage variables, ω , can be defined as

$$Y = - \frac{\delta \Psi (\varepsilon, \omega)}{\delta \omega} \quad (3)$$

which controls the kinematics of the damage evolution. To account for the nature of irreversibility during damage processes, the following criteria for damage evolution was used:

$$g_{\omega} = R(Y) - r(\omega) \quad (4)$$

where R denotes the function describing the current damage state and r denotes the damage strengthening threshold at the current time. Equation (4) can be used for modeling the initiation of the damage as well as initial damage in the material as the result of the material processing conditions. Equation (4) assumes that damage in the material evolves only during load increase.

Damage Model with Strain Tensor Split

The CSM composite can be generally considered to be isotropic in the plane of the laminate. Material anisotropy can be induced by irregularities in both CSM production (e.g. uneven fiber deposition speed) and composite manufacturing process (e.g. stretching the mat during placement). Such material property variations were not considered in this study because they have not exhibited significant influence on experimentally observed deformation.

The developed material model for CSM composite is founded in observation that microcrack evolution in the composite is primarily determined by the principal stress states and by local stress fluctuations associated with the resulting microstructure behavior. The concept of stress and strain decomposition for brittle materials modeling has been used in a number of studies for both homogeneous and composite materials, see for example References 20-26. The developed model extends the above referenced material models to impact deformation and accounts for damage processes in both tension

and compression.

The formulation of the model is based on defining the strain energy of the CSM composite in terms of principal strains as

$$\Psi = (1 - \omega_+) G \left[(\varepsilon_+ : \varepsilon_+) + \frac{4\nu}{1-\nu} (\varepsilon^m_+)^2 \right] + (1 - \omega_-) G \left[(\varepsilon_- : \varepsilon_-) + \frac{4\nu}{1-\nu} (\varepsilon^m_-)^2 \right] \quad (5)$$

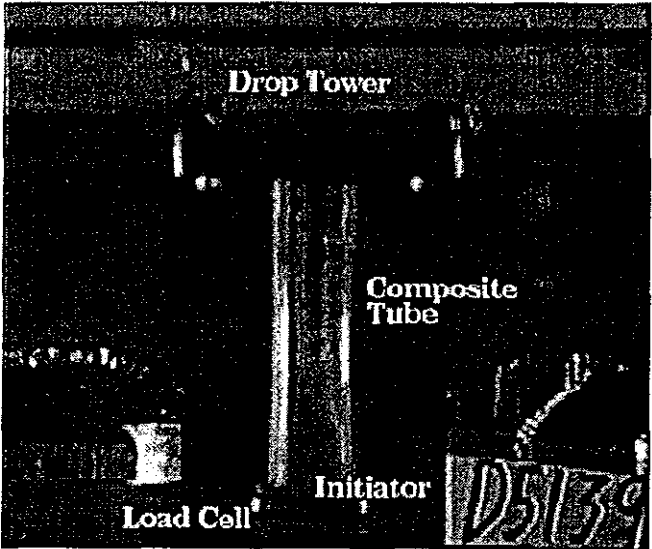
where G denotes the shear modulus of the composite, ε_+ and ε_- denote the positive and the negative part of the strain tensor, respectively. Variables ω_+ and ω_- denote the variables describing respective tensile and compression deterioration of the material with increasing load. The relations relating strain and stress and damage evolution for a given loading are derived from Eq. (5) using Eqs. (1) - (4). The damage evolution in each mode is based on the statistical distribution of flaw strengths in the material²⁷ that can be determined from uniaxial tensile and compression coupon tests.

In the case of the axial impact of tubular automotive components the compressive damage involves a number of damage processes such as fiber crushing and kinking, matrix crushing and longitudinal splitting. Tensile damage includes fiber break and pull-out, fiber-matrix debonding and matrix cracking. The multiple physical mechanisms in each mode are aggregated into a single damage variable and treated as a single process. In other words, this approach assumes that the interaction and dynamics of micromechanical processes do not significantly change during impact conditions that are being considered in this study. Computational simulations of impact geometries and loadings, for which the experimental data was available, indeed, have shown that lumping of multiple damage processes was justified. On the other hand, the advantages that this simplifying assumption has in terms of computational feasibility and conceptual simplicity are imposing limitations on the general applicability of the model. These limitations must be recognized and carefully evaluated when applying the model under different loading conditions.

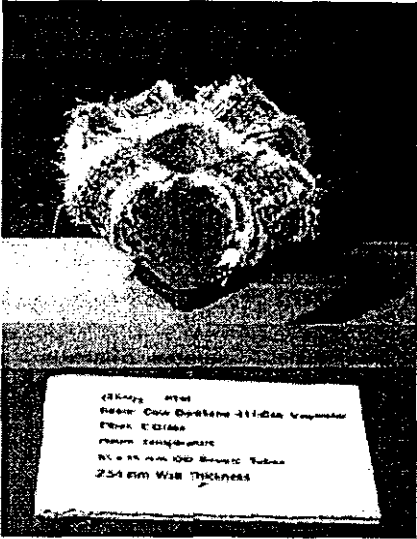
Results

The developed material model has been implemented in the computational finite element program DYNA3D. The computational model was used for simulating drop tower tests of different tube geometries and layer configurations, as well as impact of complex automotive structures. Figure 15 illustrates a typical drop tower test setup and the resulting deformed specimen. As stated earlier, the structural properties of CSM restrict the extent of possible intra- and inter-ply cracking and favor material crushing as the primary energy dissipation mechanism. Consequently, impact deformation is more unstable compared to more ordered fiber systems and accompanied with considerable material fragmentation and impact force oscillations. Results of the computational simulation using the developed material model are presented in Figure 16. The model captures the tearing along the corners of the tube and inversion of the tube into separate

fronds. The simulated resulting force on the load cell is in very good agreement with the test data. The area below the force curve is proportional to the energy that was absorbed during the crush and indicates the crashworthiness of the structure.



(a)



(b)

Figure 15 (a) Drop Tower Test of CSM Tube, (b) Deformed Tube After Test

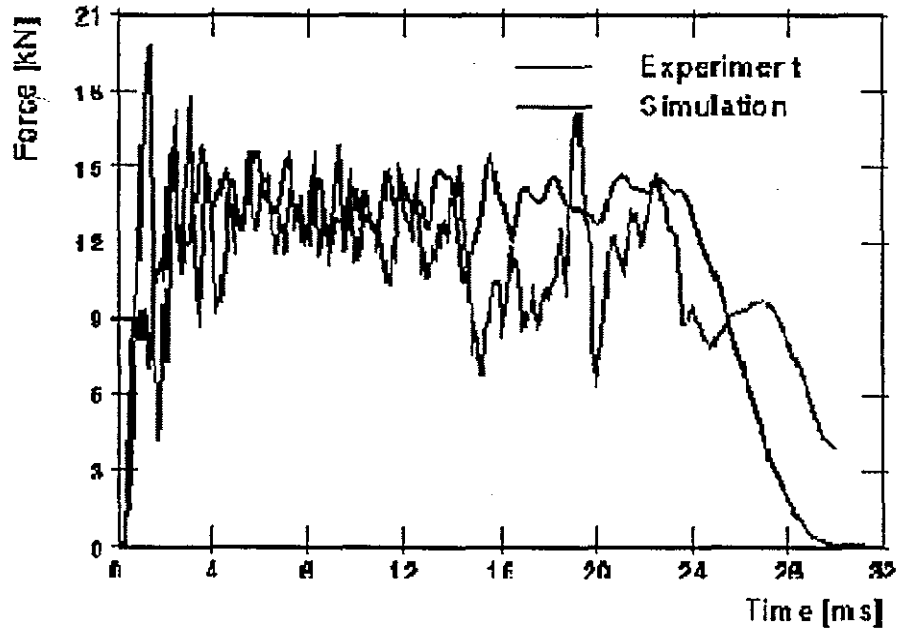
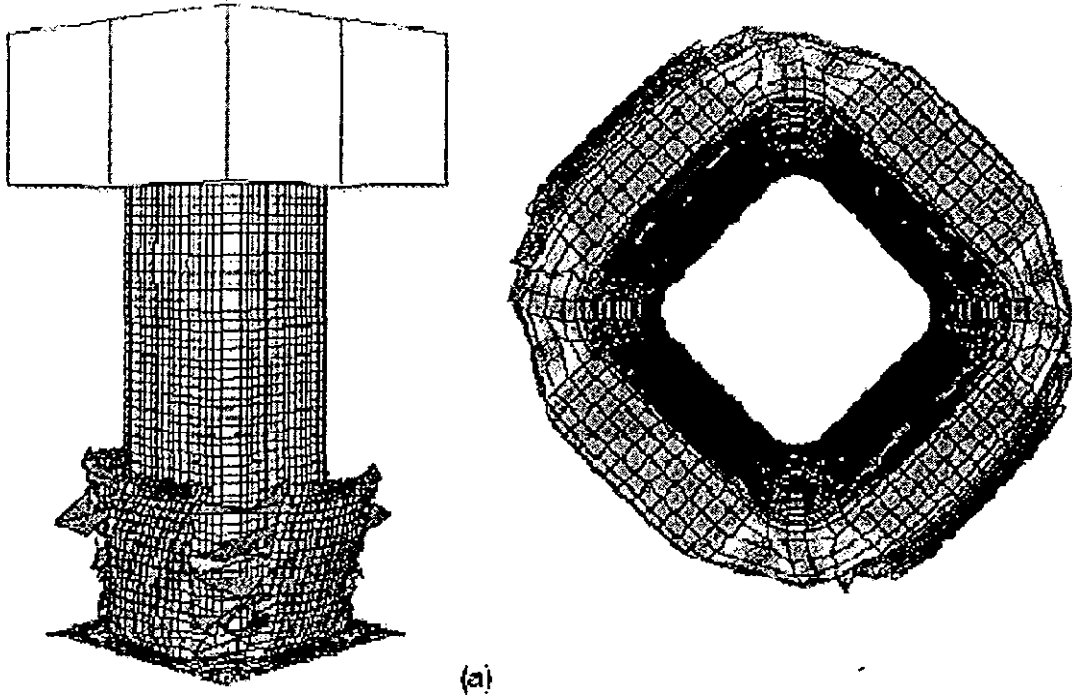


Figure 16 (a) Drop Tower Tube Crush Simulation, (b) Comparison with Test

SUMMARY

This paper summarizes the extensive amount of research that has been sponsored by the ACC since 1990 dealing with dynamic crush simulation of fiberglass composite tubes. The initial work treated tubes fabricated from hand-layed-up unidirectional material and was based upon classical damage mechanics. The results of simulation compared with drop tower tests showed good correlation in force prediction, but the deformed shape of the finite element model did not match the test results. More recent work carried out by the National Labs extended the ACC modeling capabilities to fiberglass reinforcement types typical of those used in high-volume automotive manufacturing, i.e., braided preforms and CSM material. In these cases, excellent correlation was achieved between simulation and test and the failure modes were representative of those observed in the tests. In all cases, however, the models were based upon non-physical parameters that could be used to adjust the simulation results to more closely represent the test results and therefore a truly predictive capability was not demonstrated. More work needs to be done to fully understand composite crush and to determine what material properties and models are necessary to control crash performance.

ACKNOWLEDGMENTS

The authors wish to thank the members of the Energy Management Working Group of the ACC for their efforts in providing the test data for verification of the software. In addition, special thanks should be given to Venki Agaram of Chrysler, and Sukru Fidan, formerly of Ford, for their extra effort in this activity. Portions of this research were sponsored by the U.S. Department of Energy, Assistant Secretary for Energy Efficiency and Renewable Energy, Office of Transportation Technologies, Lightweight Materials Program, and by the U.S. Department of Energy Defense Programs, Assistant Secretary, Technology Management Group, Technology Transfer Initiative, under contract DE-AC05-96OR22464 with Lockheed Martin Energy Research Corporation. Certain portions of this research were performed under the auspices of the U.S. Department of Energy by Lawrence Livermore National Laboratory under Contract W-7405-Eng-48.

REFERENCES

- 1 Dearlove, T.J., Denton, D.L., Jeryan, R.A., and Peterson, D.G., "Piecing Together Structural Technology," ESD Technology, pp. 4-7, August 1991.
- 2 Botkin, M.E., Fidan, S., and Jeryan, R.A., "Crashworthiness of a Production Vehicle Incorporating a Fiberglass-Reinforced Composite Front Structure," SAE Paper No. 971522, pp. 99-106, April 1997.
- 3 Oehmke, S.Y., "Verification of DYNA3D Failure Criteria for Glass Fiber Composite Materials," Thesis, GM Engineering and Management Institute, 1988..
- 4 Chang, F.K. and Chang, K.Y., "A Progressive Damage Model for Laminated Composites Containing Stress Concentrations," J. of Composite Materials, Vol. 21, pp. 834-855, 1987.
- 5 Botkin, M.E., Johnson, N.L., Hallquist, J., Lum, A., and Matzenmiller, A., "Numerical Simulation of Post-Failure Crushing of Composite Tubes," Second International LS-Dyna3d Conference, September 1994.
- 6 Agaram, V., et al, "Simulation of Controlled Failure of Automotive Composite Structures with LS-DYNA3D", Advanced Composites Conference and Exhibition, Detroit, MI, April 7-10, 1997.
- 7 Haug, E., Fort, O., and Tramecon, A., "Numerical Crashworthiness of Automotive Structures and Components Made of Continuous Fiber Reinforced Composite and Sandwich Assemblies," SAE Transactions Paper No. 910152, Vol. 100, pp. 245-258, 1991.
- 8 Kerth, S., et al, "Experimental Investigation and Numerical Simulation of the Crush Behavior of Composite Structural Parts," 41st International SAMPE Conference, pp. 1397-1407, March 24-28, 1996.
- 9 Belytschko, T.B. and Tsay C.S., "Explicit Algorithms for Nonlinear Dynamics of Shells", AMD-Vol. 48, ASME, 1981, p 209-231.
- 10 Belytschko, T.B., Lin, J., and Tsay, C.S., "Explicit Algorithms for Nonlinear Dynamics of Shells", Comp. Meth. Appl. Mech. Eng., 43, 1984, p 251-276.
- 11 Hallquist, J.O. and Benson, D.J., "A Comparison of an Implicit and Explicit Implementation of the Hughes-Liu Shell", Finite Element Methods for Plate and Shell Structures, Eds. Hughes, T.J.R. and Hinton, E., Pineridge Press Int., Swansea, U.K., 1986, p 394-431.

-
- 12 Hughes, T.J.R. and Liu, W.K., "Nonlinear Finite Element Analysis of Shells: Part II. Two-Dimensional Shells", *Comp. Meths. Appl. Mechs.*, 27, 1981, p 167-181.
 - 13 Hughes, T.J.R., Liu, W.K., and Levit, I, "Nonlinear Dynamics Finite Element Analysis of Shells", *Nonlinear Finite Element Analysis in Struct. Mech*, Eds. Wunderlich, Stein and Bathe, Springer-Verlag, Berlin, 1981, p 151-168.
 - 14 Matzenmiller, A., and Schweizerhof, K., "Crashworthiness Simulations of Composite Structures - A First Step with Explicit Time Integration", *Nonlinear Computational Mechanics - A State of the Art*, Eds. P. Wriggers and W. Wagner, to be published, 1991.
 - 15 Reedy, E.D., Jr., Mello, F.J., and Guess, T.R., "Modeling the Initiation and Growth of Delaminations in Composite Structures," *J. of Composite Materials*, Vol. 31, pp. 812-31, 1997.
 - 16 Hansen, N. R., and Schreyer, H. L., (1994), "A thermodynamically consistent framework for theories of elastoplasticity coupled with damage," *International Journal of Solids and Structures*, 31, pp. 359-389.
 - 17 Govindjee, S., Kay, G. J., and Simo, J. C., (1995), "Anisotropic modeling and numerical simulation of brittle damage in concrete," *International Journal for Numerical Methods in Engineering*, 38, pp. 3611-3633.
 - 18 Hill, R., (1983), *The Mathematical Theory of Plasticity*, Oxford, Oxford University Press, p. 319.
 - 19 Krajcinovic, D., *Damage Mechanics*, Elsevier, 1996.
 - 20 Ladeveze, P. and Lemaitre, J., *Damage effective stress in quasi-unilateral conditions*, Proc. IUTAM Congress, Lyngby, Danmark, 1984.
 - 21 Ortiz, M., *A constitutive theory for inelastic behavior of concrete*, *Mech. Mater.*, 4:67-93, 1985.
 - 22 Simo, J. C., Ju, J. W., *Strain- and stress-based continuum damage models*, *International Journal of Solids and Structures*, 23:821-840, 1987.
 - 23 Ladeveze, P., *A damage computational method for composite structures*, *Computers & Structures*, 44:79--87, 1992.
 - 24 Lubarda, V. A., Krajcinovic D., and Mastilovic S., *Damage model for brittle elastic solids with unequal tensile and compressive strengths*, *Engineering Fracture Mechanics*, 49:681--697, 1994.

-
- 25 Ladaveze P., Gasser A., and Allix O., Damage mechanisms modeling for ceramic composites, *Journal of Engineering Materials and Technology*, 116:331--336, 1994.
- 26 Schreyer, H. L., Continuum damage based on elastic operators, *International Journal of Damage Mechanics*, 4:171-185, 1995.
- 27 Weibull, A., A statistical distribution function of wide applicability, *Journal of Applied Mechanics*, 18:293--297, 1952.

